

# Quantum Conductance Oscillations in Metal/Molecule/Metal Switches at Room Temperature

Feng Miao,<sup>1</sup> Douglas Ohlberg,<sup>2</sup> Duncan R. Stewart,<sup>2</sup> R. Stanley Williams,<sup>2</sup> and Chun Ning Lau<sup>1,\*</sup>

<sup>1</sup>*Department of Physics and Astronomy, University of California, Riverside, California 92521, USA*

<sup>2</sup>*Information and Quantum Systems Lab, Hewlett-Packard Laboratories, Palo Alto, California 94304, USA*

(Received 19 January 2007; published 1 July 2008)

We apply pressure-modulated conductance microscopy to metal/molecule/metal switches. Apart from pressure-induced conductance peaks that indicate nanoscale conducting pathways, we also observe dips and oscillations for devices with conductance between 1 and 2 conductance quantum. The conductance oscillations arise from interfering electron waves along one or two quantum conductance channels between two partially transmitting electrode surfaces at room temperature, underscoring these devices' potential as coherent, atomic-scale switches.

DOI: 10.1103/PhysRevLett.101.016802

PACS numbers: 85.65.+h, 73.40.-c, 73.61.Ph, 73.63.-b

The formation of a point contact between two conductors provides a unique system for insight into phenomena ranging from atomic (e.g., transport in one-dimensional conductors) to macroscopic (e.g., friction and elastic properties) in scale. Extensive study has focused on electrical transport measurement of atomic point contacts created by mechanically controlled break junctions or by withdrawal of STM tips from metal surfaces [1]. Recently, atomic contacts that incorporate solid-state ionic conductors Ag and Ag<sub>2</sub>S have been proposed as the basis for nanoscale switches [2].

Here we report the reversible formation of quantum conductance channels, and evidence of quantum coherence of electrons at room temperature, in metal/molecular monolayer/metal heterostructures, whose conductances are tunable by applied voltage or current. Using the scanned probe technique of pressure-modulated conductance microscopy (PCM) [3], we observe individual nanoscale conductance dips and oscillations in response to local mechanical pressure applied by the tip of an atomic force microscope (AFM). This behavior is only observed in devices with conductance between 1 and 2 conductance quanta  $G_0$ , where  $G_0 = 2e^2/h$  or  $\approx 80 \mu\text{S}$ , indicating resonant electron transmission across quantum contacts with a few conductance channels. Our results underscore quantum coherence across the small active area responsible for switching, which can be exploited for novel nanoscale memory and logic applications.

The molecular devices consist of a Langmuir-Blodgett monolayer of stearic acid (C<sub>18</sub>H<sub>36</sub>OH) molecules sandwiched between metal electrodes. The monolayer thickness was determined by ellipsometry to be  $2.6 \pm 0.2$  nm. The bottom electrodes are 300 nm of platinum (Pt), and the top electrodes are 10–20 nm of either titanium or chromium, capped by 5 nm of Pt. Stearic acid is an electrical insulator with a band gap of  $\sim 8$  eV, and Pt/stearic acid/Pt devices do not display any conductance switching. In contrast, Pt/monolayer/Ti devices can be switched “on” and “off” by applying appropriate voltages [Fig. 1(b)]. The active switching area (or “switching centers”) are revealed by PCM [3,4], which images the device conductance while

an atomic force microscope (AFM) tip applies local mechanical pressure, thus yielding a map of the device's electrical response to local pressure [Fig. 1(a)]. Our previous work [3–5] demonstrated that when the devices are in the “on” (“off”) state, nanoscale pressure-induced conductance peaks appear (disappear) in the PCM image (Fig. 1 insets). Being the dominant conductance pathways,

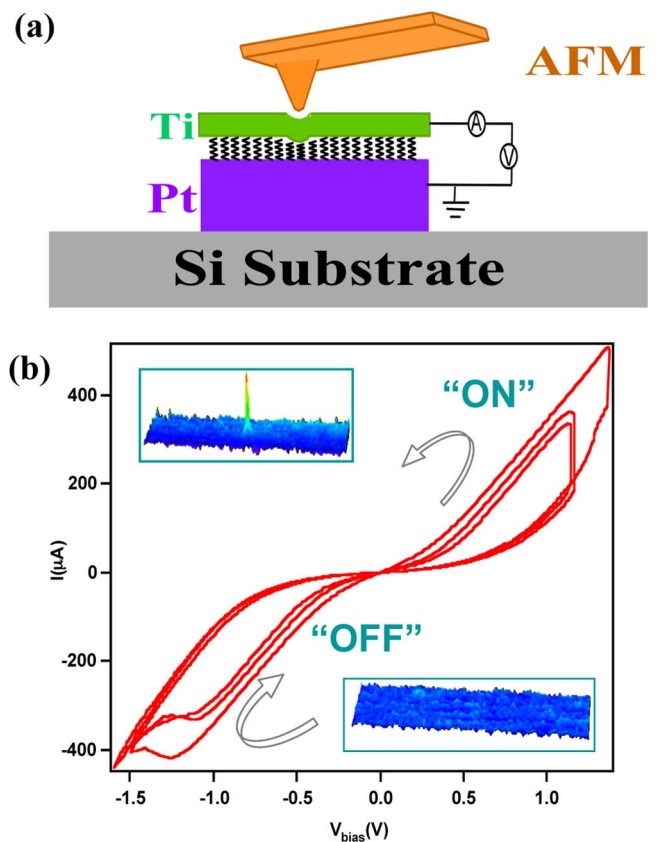


FIG. 1 (color online). (a) Experimental setup of PCM. (b) Switching characteristics of the device (arrows indicating hysteresis direction). Upper inset: a switching center appears in the PCM image when the device is switched to the “on” state. Lower inset: the switching center disappears when the device is switched to the “off” state. Scan size:  $10 \times 2.5 \mu\text{m}^2$ .

these switching centers are most simply modeled as nano-scale asperities that partially or completely bridge the electrodes.

To further investigate these switching centers, we performed PCM in more than 40 devices, and systematically examined the relative amplitude of the device's mechano-electrical response at a fixed compressive strain, parameterized by  $\Delta g = \frac{G(\varepsilon_{zz}) - G(0)}{G(0)}$ . Here  $G(\varepsilon_{zz})$  is the conductance of the device under compressive strain  $\varepsilon_{zz}$ . The results are summarized in Fig. 2, which plots  $\Delta g$  as a function of the unperturbed conductance  $G(0)$ . To estimate  $\varepsilon_{zz}$  at the electrode interfaces, we model the effect of the AFM tip using classical elasticity theory [6]. For a point force  $F$  at the origin applied to a semi-infinite elastic medium,  $\varepsilon_{zz}$  at a depth  $d$  inside the medium is approximately

$$\varepsilon_{zz}(x, y) \sim \frac{3}{2\pi E} \frac{d^3}{(x^2 + y^2 + d^2)^{5/2}} F. \quad (1)$$

Here  $E$  is the Young's modulus of the medium,  $\sim 100$  GPa for both the metals and the monolayer [7–10],  $(x, y)$  are the coordinates of the point under consideration, and  $d$  is taken to be the thickness of the top electrode. For  $F = 0.5 \mu\text{N}$  and  $d = 15$  nm, we estimate that the monolayer is compressed by 1%. For the data shown in Fig. 2, depending on values of  $d$ ,  $F$  ranges from 0.5 to 1.5  $\mu\text{N}$ , yielding  $\varepsilon_{zz}(0, 0) \sim 1\%$ .

The data points in Fig. 2 clearly fall into three regimes. For very resistive devices with  $G \ll G_Q$ ,  $\Delta g$  is relatively large,  $\sim 10\%$ – $30\%$ , whereas very conductive devices ( $G > 2G_Q$ ) have  $\Delta g < \sim 3\%$ . Both behaviors can be quantitatively understood by considering the effect of local pressure exerted on the nanoasperities. For very resistive

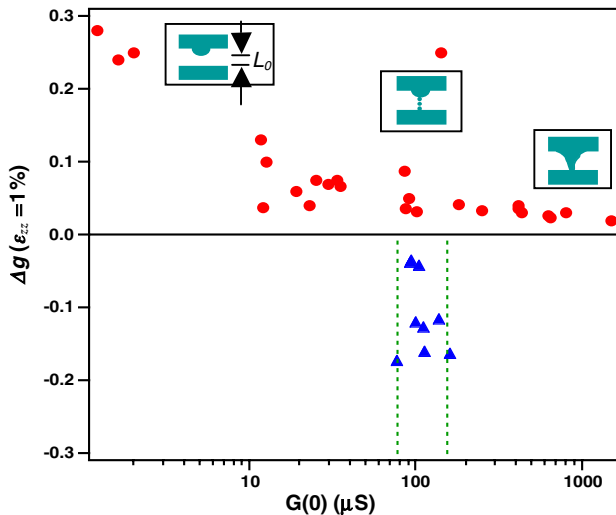


FIG. 2 (color online). Relative change in conductance under 1% strain vs  $G(\varepsilon_{zz} = 0)$ . The dotted lines denote  $G = G_Q$  and  $G = 2G_Q$ , respectively. Insets: schematic representations of microscopic atomic configurations for devices with  $G(0) \ll G_Q$ ,  $G(0) \sim G_Q$ , and  $G(0) \gg G_Q$ , respectively.

devices, we consider electrical conduction via tunneling. Generally, the tunneling conductance  $G \propto e^{-\beta L}$ , where  $L$  is thickness and  $\beta$  is a parameter that depends on the barrier height and temperature. Upon applied pressure,  $L$  is decreased from the initial value  $L_0$  by an amount

$$\delta L = L - L_0 = \varepsilon_{zz} L_0. \quad (2)$$

Thus, for devices with  $G \ll G_Q$ , the nanoasperity does not completely bridge the gap,  $\Delta g = \frac{G(L_0 - \delta L)}{G(L_0)} - 1 \approx \beta \delta L$ . Using  $L_0 \sim 2$  nm and  $\beta \approx 1/\text{\AA}$  for alkane molecules [7,11], we estimate that  $\Delta g \sim 25\%$ . This agrees well with the 10%–30% measured experimentally. On the other hand, for devices with  $G \gg G_Q$ , there are many channels with transmission coefficients  $T \sim 1$ . Hence electrical response under compression is small, arising mainly from an increase in the cross-sectional area. As the detailed configurations of the conducting pathways are not known, we can estimate the magnitude of  $\Delta g$  by modeling the conducting pathway as either (1) a ballistic point contact [1,12] with conductance  $G \approx \frac{2e^2}{h} \frac{A}{\lambda_F^2}$ , or (2) a diffusive contact with  $G = \sigma \frac{A}{L}$ . Here  $\lambda_F$  is the Fermi wavelength, and  $A$  is the total cross-sectional area. Assuming a Poisson's ratio of 0.3, both models yield  $\Delta g \sim 1\%$ , in agreement with the experimental data.

Now we focus exclusively on devices with  $G(0)$  between 80 and 160  $\mu\text{S}$ , or  $1$ – $2G_Q$ . What immediately distinguishes this regime is the observation of “inverse” switching centers, i.e., those with negative values of  $\Delta g$  that indicate *dips* in conductance in response to local pressure

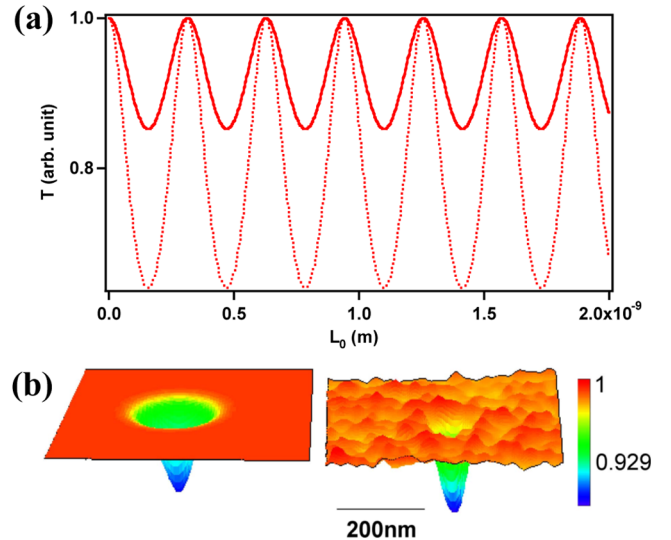


FIG. 3 (color online). (a) Periodic oscillations in  $T(L)$ , calculated using Eq. (4) and  $k_2 = 10^{10} \text{ m}^{-1}$ . Solid line:  $\gamma = 1$ . Dotted line:  $\gamma = 0.5$ . (b) Experimental data (right) and model (left) showing the conductance dip vs the tip position, with  $\varepsilon_{zz}(0, 0) = 3.8\%$ . Color scale:  $G/G(0)$ . The simulation is calculated using Eq. (4),  $\gamma = 0.5$  and  $L_0 = 1.15$  nm.

[Fig. 3(b)]. For 19 devices with  $G(0) \sim 1-2G_Q$ , we observe 9 normal and 10 inverse switching centers [13].

Such inverse switching centers, with smaller conductance under compression, are rather counterintuitive, and difficult to be explained in terms of transport across either a tunnel barrier, or across a number of highly transparent channels. The fact that inverse switching centers are found only in devices with  $G(0) \sim 1-2G_Q$  is particularly striking. It is reminiscent of the conductance parity oscillation and negative slopes observed in the final conductance plateau in metal point contacts formed by mechanically controlled break junctions (MBJ) [1,14–16]. Our data thus suggest the formation of one or two highly transmitting quantum conductance channels between the top and bottom electrodes. These channels may be a linear chain of atoms (i.e., a metal point contact), or perhaps a column of aligned oxygen deficiency sites in titanium oxide [17–19]. Upon applied pressure, the atoms undergo rearrangement, altering the transmission coefficient  $T$  of the conductance channel(s). Such conformation-induced change in  $T$  may take place via a number of atomic configurations such as changes in orbital overlap. Here we adopt a simple phenomenological model to aid our quantitative understanding of the data: we assume the conducting channels bridging between the electrodes form a small Fabry-Perot cavity for electrons, which remain phase coherent at room temperature for such short length scales [20]. As electron waves propagate through the channel between two partially reflecting barriers, the incoming and multiply reflected electron paths interfere and give rise to periodic oscillations in the transmission coefficient as a function of interelectrode spacing. The barriers may be the electrode interfaces or impurities in close proximity.

Quantitatively, by matching the boundary conditions of a 1D wave function of a particle propagating through two barriers,  $T$  is given by [15]

$$T = \frac{16\gamma^2}{(1 + \gamma)^4 + (1 - \gamma)^4 - 2(1 + \gamma)^2(1 - \gamma)^2 \cos(2k_2L)}, \quad (3)$$

where  $\gamma = k_2/k_1$ ,  $L$  is the length of the channel,  $k_2$  is the wave vector in the conducting channel, and  $k_1$  in the electrodes. Here, importantly, we treat  $k_2$  and  $L$ , as independent variables; i.e., we assume that  $k_2$  is a material parameter of the conductance channel, and that  $L$  is an independent and continuous variable. Also, for simplicity we assume that the electrons in the two electrodes have the same wave vector (different wave vectors will modulate the absolute values of  $T$ ). The resulting graph is a periodic function of  $L$ , as plotted in Fig. 3(a), using reasonable parameters for metals,  $k_2 = 10^{10} \text{ m}^{-1}$ ,  $\gamma = 1$  (solid lines), and  $\gamma = 0.5$  (dotted lines), respectively. Thus, as the compressive pressure from the AFM tip decreases  $L$ ,  $T$  can either increase or decrease, depending on the initial value of  $L$ .

To simulate the conductance dips in the PCM images, we substitute Eqs. (1) and (2) into (3) to obtain  $T$  as a function of tip position  $(x, y)$ . Assuming 1-channel transmission and taking into account electron spin, we have

$$G(x, y) = (2e^2/h)T(x, y). \quad (4)$$

Assuming the initial length is  $L_0 = 1.2 \text{ nm}$ , the resultant conductance (4) is plotted in Fig. 3(b). The resemblance between the data and the simulation is satisfactory. This simple model can thus adequately explain our observation of the inverse switching centers.

A crucial test of this model occurs in the case that the initial length  $L_0$  only slightly exceeds the value corresponding to a local transmission minimum or maximum. We then expect to observe conductance *oscillations* with increasing pressure: as the AFM tip approaches the conducting channel,  $L$  decreases, reaching a minimum at the center, then increases as the tip moves away; thus  $T(L)$  will pass through the local extremum before reversing slope. Such conductance oscillations would appear as rings in the PCM image. Indeed, these rings are observed in four of the devices with conductance  $G \sim 1-2G_Q$  (but not in those with  $G \gg G_Q$  or  $G \ll G_Q$ ). Both “W”-shaped (i.e., with a center peak, Fig. 4(a), left panel) and “M”-shaped (i.e., with a center dip, Fig. 4(b), left panel) ring are observed, corresponding to a local minimum and maximum in  $T(L)$ , respectively. We can simulate these features with our simple model, by using  $L_0 = 1.45 \text{ nm}$  and  $L_0 = 1.59 \text{ nm}$ , respectively [Figs. 4(a) and 4(b), right panels].

A rather dramatic prediction of this model is the ability to manipulate the shape of the switching center response by modulating the applied pressure. For one device with  $G_Q < G < 2G_Q$ , we succeeded in this shape manipulation. At  $\epsilon_{zz} \sim 2.4\%$ , the device displayed an inverse switching center, with  $\Delta g \sim -12\%$  (cross section in Fig. 4(c), top panel). Remarkably, when imaged at an increased strain of 6.5%, the exact same switching center appeared with oscillations as a “W”-shaped ring [Fig. 4(c), bottom panel]. We note that we are able to compress the length of the quantum conductance channel by up to  $\sim 6\%$  to produce the conductance oscillations. In principle, similar modulation may also be produced by applying higher voltage bias to populate higher  $k$  states in the channel. However, such a level of manipulation requires application of bias voltage of  $\sim 0.5-1 \text{ V}$ ; yet at such high voltages, undesirable effects, such as Joule heating and electromigration, are expected to emerge and destabilize the contact. This is borne out in experiment, where these voltages are high enough to induce atomic reconfiguration, i.e., electrical switching [Fig. 1(b)]. A unique advantage of the PCM technique is therefore a relatively large quantum modulation that enables investigation of quantum processes at room temperature without destabilizing the contact.

Finally, we note that even though the phenomenological model of partially reflected electron waves is likely not a

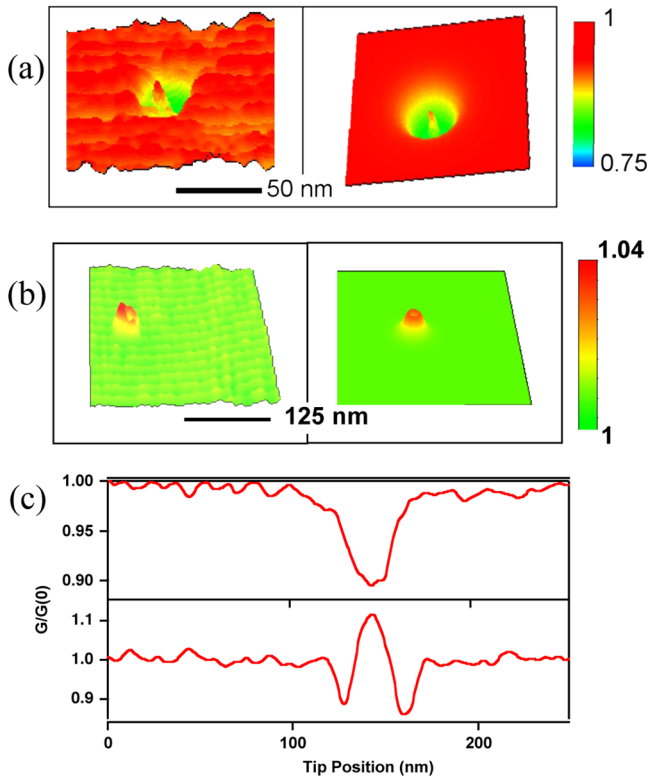


FIG. 4 (color online). PCM images of conductance oscillations. Color and vertical scale:  $G/G(0)$ . (a)  $W$ -shaped oscillation. Left panel: data taken at  $\varepsilon_{zz}(0,0) = 6\%$ . Right panel: Simulation calculated using Eq. (4),  $\gamma = 0.5$  and  $L_0 = 1.45$  nm. (b)  $M$ -shaped oscillation. The data are taken at  $\varepsilon_{zz}(0,0) = 2\%$ , and simulation calculated using  $\gamma = 0.5$  and  $L_0 = 1.59$  nm. (c) Line traces through experimental data from a switching center at different compressive strains:  $\varepsilon_{zz}(0,0) = 2.4\%$  (upper) and  $6.5\%$  (lower trace).

unique model, it is a simple yet effective aid at understanding our data presented in Figs. 2–4. For instance, a model of changes in orbital overlap of atoms may predict certain phenomena such as smaller conductance under compression; yet, to explain the observation of *both* “ $M$ -shaped” and “ $W$ -shaped” conductance oscillations as shown in Figs. 4(a) and 4(b), or the manipulation of the inverse switching center into a “ $W$ -shaped” ring by further compression [Fig. 4(c)], the mechanisms of orbital overlap need to invoke particular assumptions of detailed atomic arrangements. The partially reflected wave model, by comparison, offers a simple explanation with only two adjustable parameters—indeed, our observations in Figs. 2–4 are a natural conclusion arising from the oscillatory dependence of the transmission coefficient on inter-electrode spacing.

In conclusion, pressure-modulated conductance microscopy has revealed conductance peaks, dips, and oscillations in metal/molecular monolayer/metal junction devices. These phenomena can be explained by interfering electron waves within quantum conductance channels in the device. Recent experimental and theoretical studies indicate that such channels are likely asperities or oxygen deficiency sites in  $\text{TiO}_x$  layers [19,21], and their formation and dissolution mechanisms are currently under investigation. The quantum nature of these devices indicates that the active switching area is atomic in scale, and suggests that this class of junction device can be shrunk almost to the atomic limit for possible future ultrascaled coherent memory and logic applications.

We thank M. Bockrath and A. M. Bratkovsky for stimulating discussion. Work at HP was supported in part by DARPA. C.N.L. acknowledges the support of ONR/DMEA grant No. H94003-07-2-0703.

\*lau@physics.ucr.edu

- [1] N. Agrait, A.L. Yeyati, and J.M. van Ruitenbeek, *Phys. Rep.* **377**, 81 (2003).
- [2] K. Terabe *et al.*, *Nature (London)* **433**, 47 (2005).
- [3] C.N. Lau *et al.*, *Nano Lett.* **4**, 569 (2004).
- [4] C.N. Lau *et al.*, *Appl. Phys. A* **80**, 1373 (2005).
- [5] D.R. Stewart *et al.*, *Nano Lett.* **4**, 133 (2004).
- [6] E.M. Lifshitz and L.D. Landau, *Theory of Elasticity* (Butterworth-Heinemann, London, 1959), 3rd ed.
- [7] D.J. Wold and C.D. Frisbie, *J. Am. Chem. Soc.* **123**, 5549 (2001).
- [8] Y.S. Leng and S.Y. Jiang, *J. Chem. Phys.* **113**, 8800 (2000).
- [9] A.B. Tutein, S.J. Stuart, and J.A. Harrison, *J. Phys. Chem. B* **103**, 11357 (1999).
- [10] D.L. Patrick *et al.*, *J. Am. Chem. Soc.* **125**, 6762 (2003).
- [11] D.J. Wold and C.D. Frisbie, *J. Am. Chem. Soc.* **122**, 2970 (2000).
- [12] A.M. Bratkovsky and S.N. Rashkeev, *Phys. Rev. B* **53**, 13 074 (1996).
- [13] Data from a few devices are not taken at  $\varepsilon_{zz} = 1\%$  and thus not shown in Fig. 2.
- [14] J.M. Krans *et al.*, *Phys. Rev. B* **48**, 14 721 (1993).
- [15] R.H.M. Smit *et al.*, *Phys. Rev. Lett.* **91**, 076805 (2003).
- [16] J.C. Cuevas *et al.*, *Phys. Rev. Lett.* **81**, 2990 (1998).
- [17] E. Yagi, R.R. Hasiguti, and M. Aono, *Phys. Rev. B* **54**, 7945 (1996).
- [18] M. Aono and R.R. Hasiguti, *Phys. Rev. B* **48**, 12 406 (1993).
- [19] J.J. Blackstock *et al.*, *J. Am. Chem. Soc.* **130**, 4041 (2008).
- [20] B.L. Altshuler, A.G. Aronov, and D.E. Khmel'nitsky, *J. Phys. C* **15**, 7367 (1982).
- [21] D.B. Strukov *et al.*, *Nature (London)* **453**, 80 (2008).